Electron-Nuclear Hyperfine Interactions of $^{53}Cr^{3+}$ in Mg_2SiO_4 (Forsterite)

H. Rager

Department of Geosciences, University of Marburg

Z. Naturforsch. **35a**, 1296–1303 (1980); received October 25, 1980

The magnetic hyperfine interaction between the electron and nuclear spin system of $^{53}Cr^{3+}$ was studied at the Mg sites, M1 and M2, in Mg_2SiO_4. The study was undertaken at room temperature and 9.52 GHz. The hyperfine structure data exhibit a covalent Cr–O bonding of approximately 10% indicating a mainly but not purely ionic bonding. Including the corresponding results obtained for $^{57}Fe^{3+}$ [1] and $^{55}Mn^{2+}$ [2] in Mg_2SiO_4, this is interpreted such that the bonding of transition metal ions is mainly dominated by the oxygen sublattice in Mg_2SiO_4 and less by the properties of the transition metal ions themselves. The small variation of the hyperfine splitting parameters found for $^{53}Cr^{3+}$ at M1 and M2, and also for $^{57}Fe^{3+}$ at these positions indicates that the hyperfine interaction varies also with varying average metal oxygen distances as well as with changes in the oxygen coordination size.

I. Introduction

Electron spin resonance (ESR) investigations of the paramagnetic impurity ions, Fe^{3+} [1], Mn^{2+} [2], and Cr^{3+} [3] in forsterite, Mg_2SiO_4, have primarily dealt with the fine structure (FS) terms, B_k^m, which can be obtained by fitting an appropriate effective spin Hamiltonian operator to the observed ESR transitions. The hyperfine interaction between the electron and nuclear spin system of the isotopes ^{57}Fe, ^{55}Mn, and ^{53}Cr was also measured. However, there is so far no general discussion of the hyperfine structure (HFS) data with respect to the properties of the positions substituted by the above ions in Mg_2SiO_4. Therefore, in this paper we present our investigation of the $^{53}Cr^{3+}$-HFS-interaction. The results will be compared with corresponding studies of $^{57}Fe^{3+}$ [1] and $^{55}Mn^{2+}$ [2] in the forsterite crystal.

II. Crystal Structure

The well known structure of Mg_2SiO_4 [4] is illustrated in Figure 1. It can be described as being based on an approximately hexagonal, tightly-packed array of oxygens with silicon in the fourfold and Mg in the sixfold oxygen coordinated sites.

The unit cell belongs to the space group Pbnm and contains two inequivalent Mg sites, 4a and 4c, which are designated as M1 and M2, respectively. The two Mg sites differ in point symmetry which is $\bar{1}$ at 4a(M1) and m at 4c(M2), and in the sixfold oxygen coordination where the average M1-O and M2-O distance is 2.095 Å and 2.132 Å, respectively. Silicon occurs at 4c(Si) and oxygen at positions 4c(O1 and O2) and 8d(O3) where at 8d the point symmetry is 1.

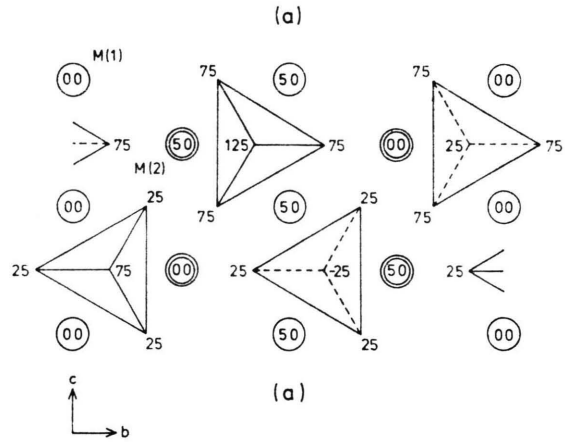

Fig. 1. Crystal structure of forsterite. The representation of the space group is Pbnm. The numbers give the x-coordinate in percent of the lattice constant a (after [1]).

III. Theory

The spin Hamiltonian operator which describes the ground state energy levels of the paramagnetic impurities $^{57}Fe^{3+}$, $^{55}Mn^{2+}$, and $^{53}Cr^{3+}$ in a crystalline environment with an external magnetic field $\boldsymbol{H}$

Reprint requests to Dr. H. Rager, Fachbereich Geowissenschaften, Philipps-Universität Marburg, Lahnberge, D-3550 Marburg.

0340-4811 / 80 / 1200-1296 $ 01.00/0. — Please order a reprint rather than making your own copy.

is [5]

$$\hat{H} = \beta \boldsymbol{H} \mathbf{g} \boldsymbol{S} + \sum_{m=-2}^{+2} B_2^m O_2^m + \sum_{m=-4}^{+4} B_4^m O_4^m + \boldsymbol{S} \mathbf{A} \boldsymbol{I}^* . \quad (1)$$

The first term describes the Zeeman interaction between the effective electron spin $\boldsymbol{S}$ and the applied magnetic field $\boldsymbol{H}$. The second and third terms depend on the second and fourth derivatives, respectively, of the crystal field potential at the substitutional site. They are called fine structure (FS) terms and stand for the interaction of the effective electron spin $\boldsymbol{S}$ with the electric field derivatives at the paramagnetic center. In the fourth term the tensor $\mathbf{A}$ represents the hyperfine interaction between the electron (S) and the nuclear (I) spin of the paramagnetic ion. For a predominantly orthorhombic environment the fourth term can be written [6] as

$$\boldsymbol{S} \mathbf{A} \boldsymbol{I} = A S_z I_z + B(S_x I_x + S_y I_y) . \quad (2)$$

A and B will, in general, be made up of contributions from the orbital, spin dipolar, and Fermi contact interactions. They depend on the ion itself and in particular on the ground state of the ion under investigation.

The electron configuration of Fe^{3+} and Mn^{2+} is $[Ar]3d^5$ and of Cr^{3+} $[Ar]3d^3$ where [Ar] denotes the electron configuration of the noble gas argon. In the high spin state these configurations result in an orbital singlet i.e., the orbital momentum L of Fe^{3+}, Mn^{2+}, and Cr^{3+} is quenched or, in other words, the expectation value of L is zero. Then, the ground state hyperfine interactions are almost entirely due to the contact and spin-dipolar terms. However, spin-orbit coupling either by itself or in conjunction with low-symmetry crystal field matrix elements mixes in excited states, thereby reintroducing an orbital contribution into A and B.

The same mixing carries the electron g shift from 2.0023, and one can often write the orbital hyperfine terms [6] as

$$A_{\text{orb}} = 2.0023\, g_I \mu_0 \mu_I \Delta_{g\parallel} \langle r^{-3} \rangle , \quad (3.1)$$

$$B_{\text{orb}} = 2.0023\, g_I \mu_0 \mu_I \Delta_{g\perp} \langle r^{-3} \rangle . \quad (3.2)$$

$\Delta_{g\parallel}$ and $\Delta_{g\perp}$ are the parallel and perpendicular electron g shifts. μ_0 and μ_I are the Bohr and nuclear magnetons. g_I is the nuclear spectroscopic splitting factor and $\langle r^{-3} \rangle$ refers to the 3d orbitals of the paramagnetic ion under investigation. Provided there are no contributions which arise from electron transfer or high order effects, (3.1) and (3.2) will supply accurate estimates of the orbital hyperfine contribution to A and B.

If the hyperfine interaction is assumed to be mainly isotropic, i.e. $A \gg B$, the relation

$$H^{\text{HF}} = A S / g_I \mu_I \quad (4)$$

approximately determines the magnetic hyperfine field H^{HF} at the nuclear site [7]. Experimental and theoretical estimates show that for $3d^n$ ions the normalized hyperfine field $H^{\text{HF}}/2S$ is roughly constant for ions of common valency in common environments. Significant deviations from the constancy are assigned to covalent contributions in the metal-ligand bonding. Therefore, the investigation of the hyperfine interaction is one method to obtain information on the covalency of the metal-ligand bonding [8].

IV. Experimental Results and Discussion

Due to the hyperfine interaction, the ESR fine structure lines of Fe^{3+} and Cr^{3+} are centered by $2I+1$ approximately equally spaced hyperfine structure (HFS) lines (Fig. 2) where I is the nuclear spin of the isotopes ^{57}Fe and ^{53}Cr. The intensity of the HFS lines results from the abundant transition metal isotopes with a nuclear spin I. For example, in the case of the chromium doped forsterite the Cr-HFS-intensity is roughly 10% according to the 9.42% natural abundant ^{53}Cr isotope with $I = 3/2$. For Mn^{2+} only HFS lines exist (Fig. 2a) because of the 100% abundant ^{55}Mn isotope. The HFS lines of $^{57}Fe^{3+}$, $^{55}Mn^{2+}$, and $^{53}Cr^{3+}$ in Mg_2SiO_4 are well resolved. Their overall splitting ranges from 450 G for $^{55}Mn^{2+}$ via 60 G for $^{53}Cr^{3+}$ to only 13 G for $^{57}Fe^{3+}$ as shown in Figures 2a–c.

The hyperfine interaction between the nuclear spin ($I=3/2$) and the effective electron spin ($S=3/2$) of $^{53}Cr^{3+}$ in forsterite was studied at room temperature and 9.52 GHz. The four hyperfine lines are well resolved (Fig. 2c) and their splitting, ΔH, depends on the crystal orientation with respect to the applied external magnetic field (Figure 3). At M2 positions the angle dependence of ΔH is small, whereas at M1 positions it is very distinct. Thus,

* For brevity the interaction of the nuclear spin $\boldsymbol{I}$ with the external magnetic field $\boldsymbol{H}$ as well as the quadrupole interaction have been omitted in Equation (1).

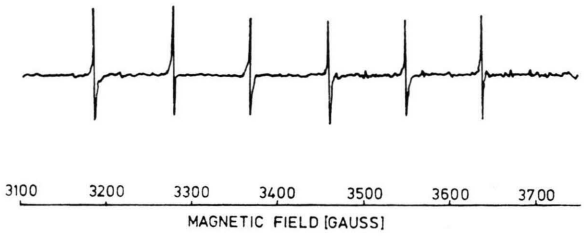

Fig. 2a. Hyperfine splitting of $^{55}Mn^{2+}$ in chromium doped forsterite. The spectrum was taken at room temperature and 9.527 GHz. The crystal was oriented with $a \perp H_0$.

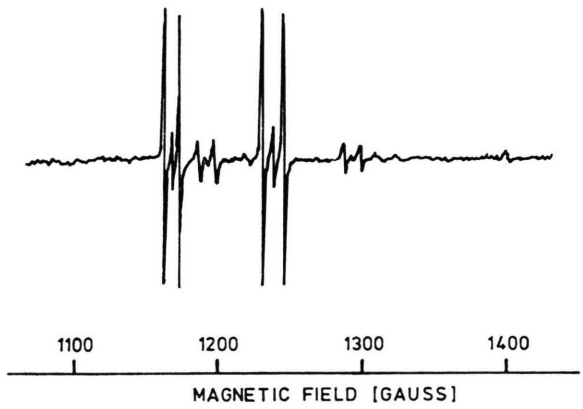

Fig. 2b. Hyperfine splitting of $^{57}Fe^{3+}$ in iron doped forsterite enriched with approximately 90% ^{57}Fe. The spectrum was taken at room temperature and 9.527 GHz. The small central lines are due to the ESR transitions of $^{56}Fe^{3+}$ with $I=0$. The crystal was oriented with $a \perp H_0$.

Fig. 2c. Hyperfine splitting of natural abundant ^{53}Cr at M1 and M2 positions in Cr doped forsterite. ΔH denotes the total HF splitting. The notations (1—2) and (3—4) indicate the Cr^{3+}-fine structure transitions $M_S = 3/2 \rightarrow M_S = 1/2$ and $M_S = -1/2 \rightarrow M_S = -3/2$, respectively. The crystal was oriented with $a \perp H_0$ and $c \| H$ (see Fig. 4).

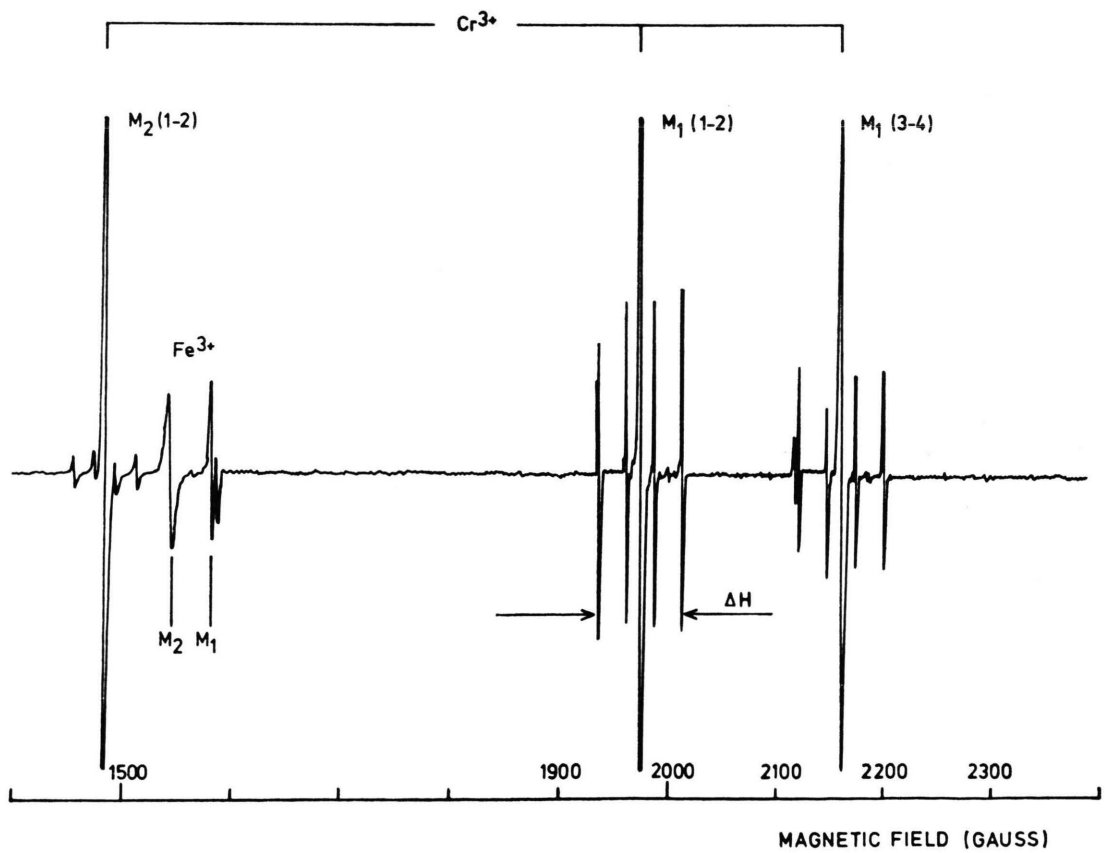

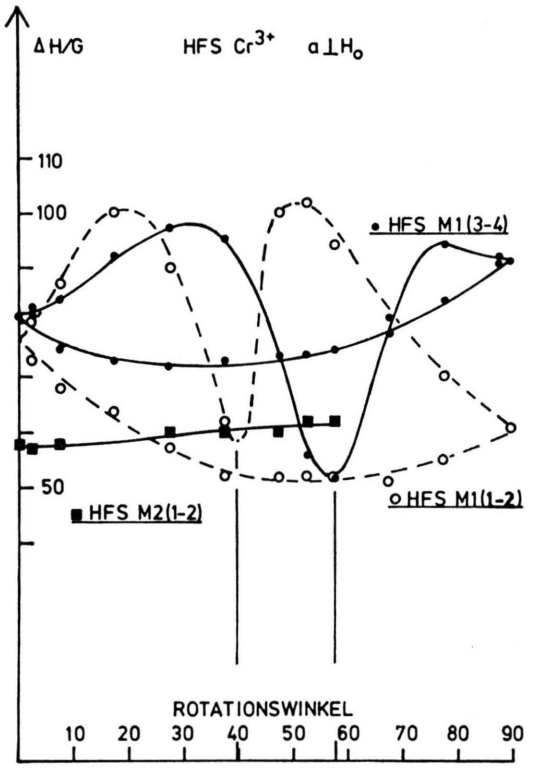

Fig. 3. Angle dependence of the $^{53}Cr^{3+}$ hyperfine splitting ΔH at M1 and M2. The crystal was oriented with $a \perp H_0$. The notations (1—2) and (3—4) are as in Figure 2c.

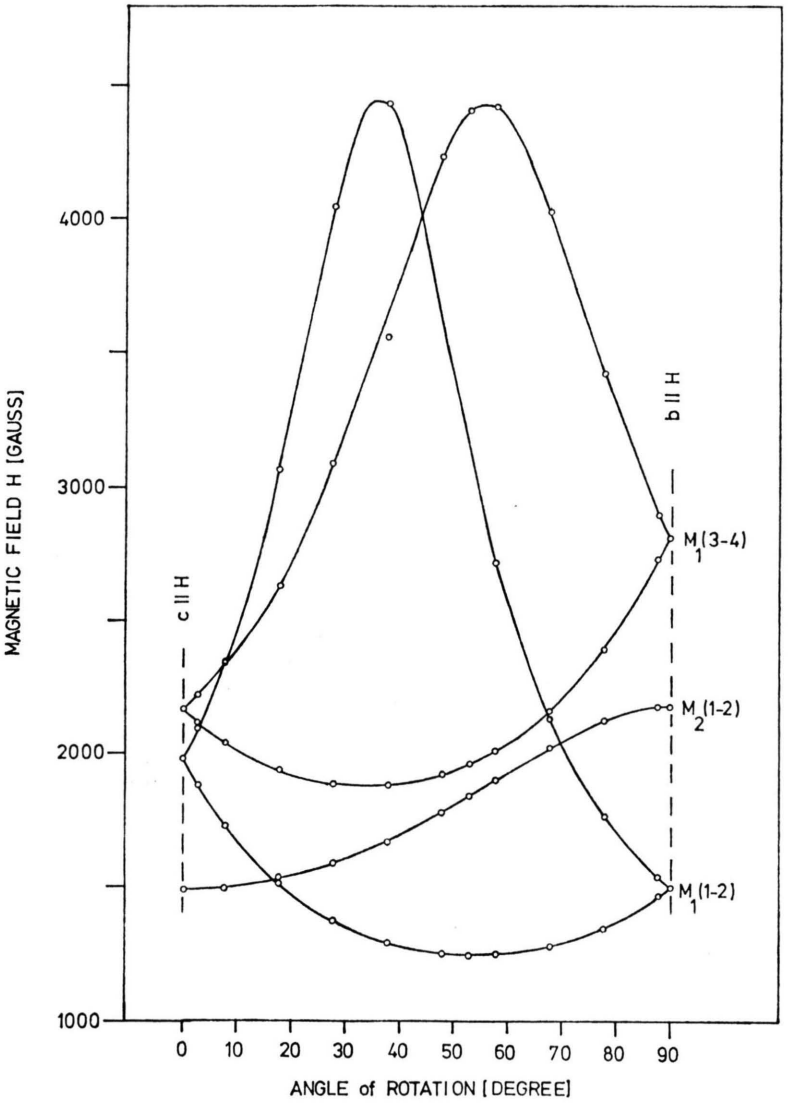

Fig. 4. Angle dependence of the Cr^{3+} fine structure ESR-transitions at M1 and M2. The notation is the same as in Fig. 2c and Figure 3.

in the following we will discuss the hyperfine splitting of $^{53}Cr^{3+}$ at M1 positions in more detail.

Comparing the rotation pattern of ΔH in Fig. 3 with that of the ESR fine structure transitions in Fig. 4, it is apparent that the angles for the maximum magnetic resonance fields, $H_{res,max}$, agree well with the angles for the minimum hyperfine splitting ΔH_{min}. The angles refer to the crystal axes system and are listed in Table 1. To understand the reason for this we transformed, by example of the Cr^{3+}(1—2) ESR transitions, the magnetic resonance field H_{res} from the crystal axes system into the principal axes system of the crystal field tensor at the Cr(M1) site (Table 2). Plotting both axes systems together in a sterographic projection, from Fig. 5 and Table 2, it can easily be seen that at the distinct crystal orientation $\sphericalangle(b, H_{res}) \approx 39°$ the z-component of the applied magnetic resonance field runs through zero in the principal axes system, whereas in the crystal axes system H_{res} runs through a maximum.

Table 1. Angles between the applied magnetic resonance field H_{res} and one crystal axis at which H_{res} for the Cr^{3+}(M1) ESR transition is at a maximum and the respective $^{53}Cr^{3+}$ hyperfine splitting ΔH at a minimum. $a \perp H_0$, $b \perp H_0$, and $c \perp H_0$ are the different crystal orientations. (1—2) and (3—4) denote the ESR fine structure transitions as in Figs. 2c, 3 and 4.

Crystal orientation	Angles between the applied maximum magnetic resonance fields, $H_{res,max}$ of the Cr^{3+}(M1) ESR transitions and one crystal axis	
Transition	(1—2)	(3—4)
$a \perp H_0$	35	55
$b \perp H_0$	8	58
$c \perp H_0$	3	68
	Angles of the corresponding minimum hyperfine splitting ΔH_{min}	
$a \perp H_0$	39	55
$b \perp H_0$	4	58
$c \perp H_0$	0	68

Table 2. Angle dependence of the normalized components of the applied magnetic resonance field, H_{res}, in the principal axes system X, Y, Z of the Cr^{3+} crystal field tensor at M1. The crystal orientation was $a \perp H_0$.

Angle	Normalized components of the applied magnetic resonance field, H_{res}, for the Cr^{3+} (1—2) ESR transitions in the principal axes system X, Y, Z of the Cr^{3+} crystal field tensor at M1.			
	X	Y	Z	Notation of the Z-component in Figure 5
0.0	0.6325	0.5077	−0.5849	□
2.8	0.6552	0.5235	−0.5447	□
7.8	0.6918	0.5485	−0.4695	□
17.8	0.7490	0.5859	−0.3091	□
27.8	0.7835	0.6056	−0.1394	□
37.8	0.7941	0.6068	−0.0345	□
57.8	0.7434	0.5545	+0.3741	×
67.8	0.6843	0.5031	+0.5278	×
77.8	0.6030	0.4352	+0.6685	×
87.8	0.5029	0.3537	+0.7885	×
89.8	0.4802	0.3355	+0.8204	×

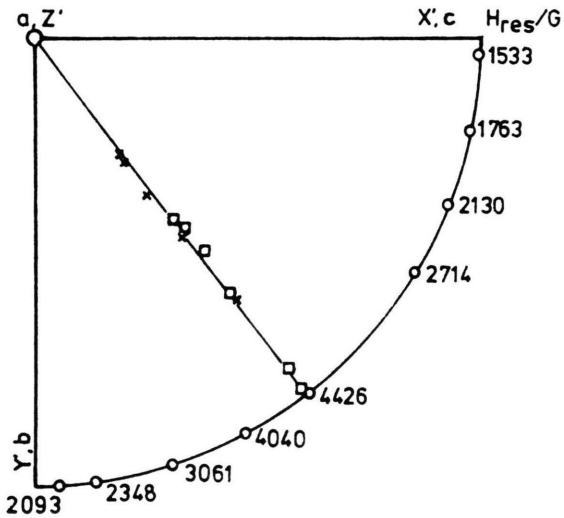

Fig. 5. Stereographic projection of the applied magnetic resonance field H_{res} in the crystal axes system a, b, c and of the z-component of H_{res} in the principal axes system X, Y, Z, of the Cr(M1) crystal field tensor (see also Table 2).

For a constant magnetic field of $H_0 = 1980$ G, the FS energy levels $E_{FS}(1)$ and $E_{FS}(2)$ were calculated by solving the corresponding energy matrix of Equation (1) [3]. The difference between $E_{FS}(1)$ and $E_{FS}(2)$ runs through a minimum at the same orientation $\sphericalangle(b, H_0) \approx 39°$. This is shown in Figure 6. Therefore, it is plausible that at this particular crystal orientation, with respect to the applied magnetic field vector, the magnetic resonance field must be raised in order to fulfill the resonance condition for the used microwave frequency of 9.527 GHz. The HF-splitting, ΔE_{HF}, of the FS-ESR levels, $E_{FS}(1)$ and $E_{FS}(2)$, is also angle dependent and at a minimum at the special angle setting of approximately 39°. This is shown in Figure 7. Thus, the hyperfine-split $^{53}Cr^{3+}$(1—2)-ESR-transitions occur near 39° very close to the hypothetic fine structure $^{53}Cr^{3+}$(1—2)-ESR-transitions yielding a minimum hyperfine splitting in accordance with the experimental results. Discussing the Cr^{3+}(3—4)-ESR-

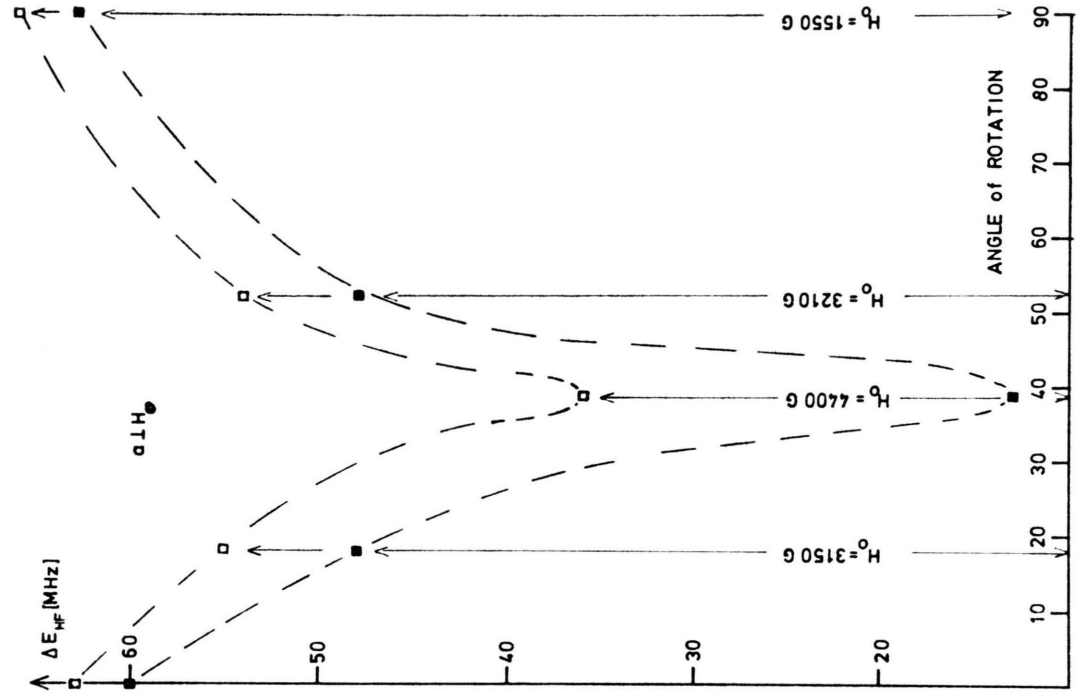

Fig. 7. Angle dependence of the hyperfine splitting, ΔE_{HF}, of the fine structure energy levels $E_{FS}(1)$ and $E_{FS}(2)$ denoted by □ and ■, respectively, for $^{53}Cr^{3+}$ at M1. The splitting was calculated using the magnetic resonance fields of the Cr^{3+} ESR fine structure transitions (see Figure 4).

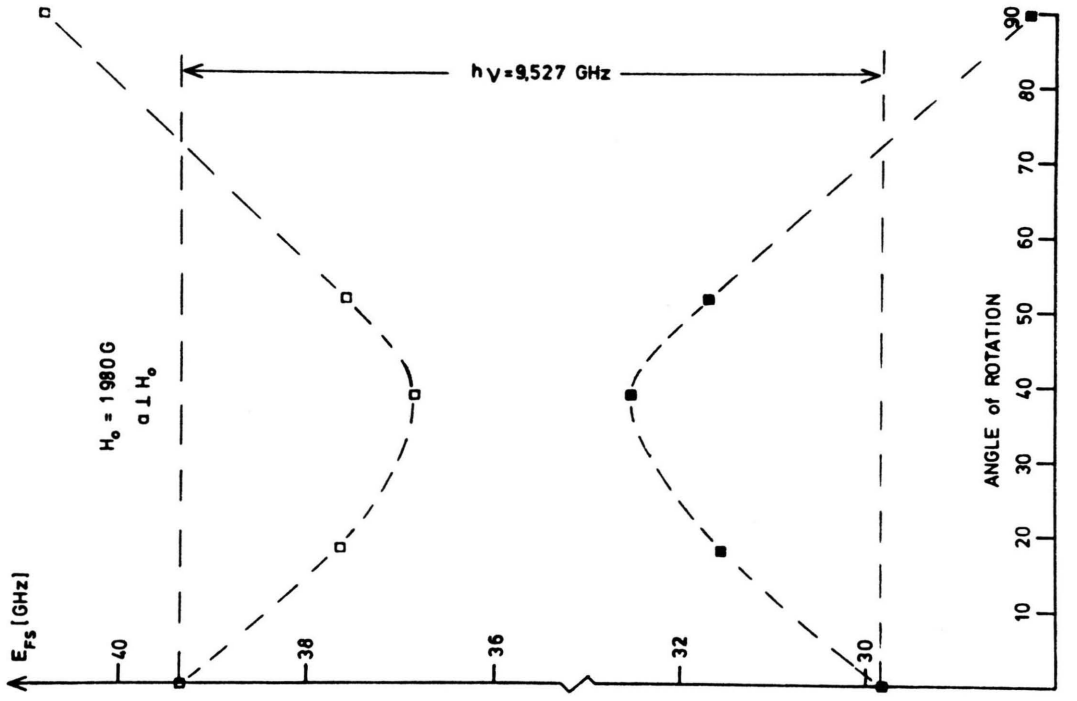

Fig. 6. Angle dependence of the calculated fine structure energy levels $E_{FS}(1)$ and $E_{FS}(2)$ denoted by □ and ■, respectively, for Cr^{3+} at M1. The crystal orientation was $a \perp H_0$. For the calculation a constant magnetic field of $H_0 = 1\,980$ G was taken.

transitions the same results will be obtained. Thus, the tensors **g** and **A** in Eq. (1) can be considered to be collinear [9] and it is justified to calculate the hyperfine constants by solving the energy matrix which was constructed of Eqs. (1) and (2).

The hyperfine constants, A and B, thus obtained for $^{53}Cr^{3+}$ at M1 and M2 positions revealed $A \gg B$ in accordance with the assumed collinearity of the tensors **g** and **A** which means that the electron and nuclear moments are aligned along the main symmetry axis of the crystal field tensor. Therefore, the ^{53}Cr hyperfine interaction is denoted by the hyperfine splitting parameter A, which is listed in Table 3. The limit of error of A at M1 and M2 is relatively large. This is due to the experimental inaccuracy in determining the magnetic resonance fields for the hyperfine transitions.

The contributions to the Cr^{3+} HF field are mainly due to the orbital and core polarization HF fields. According to the experimental result $A \gg B$ the crystalline field may be assumed to be nearly cubic and, thus, the dipolar contribution to the HF field should be negligible [5]. The orbital HF field can be estimated by the relation

$$H_{\mathrm{orb}}^{\mathrm{HF}} = 2.0023\,\mu_B S\,\Delta g_{\mathrm{av}}\langle r^{-3}\rangle \qquad (5)$$

if Δg is entirely due to orbital effects and isotropic. For $3d^3$ ions the normalized orbital HF field $H_{\mathrm{orb}}^{\mathrm{HF}}/2S$ is small in comparison to the HF field produced by the core polarization effect [5]. It varies with the metal-oxygen distance in such a way that the orbital HF field increases with increasing M–O distance. Assuming an isotropic g-shift from 2.0023, we may estimate from the eigenvalues of the Cr^{3+}-g-tensor at M1 and M2 [3] that $\Delta g_{\mathrm{av}} \approx 0.031$ and $\Delta g_{\mathrm{av}} \approx 0.041$, respectively. From Eq. (5) we then obtain a larger orbital field at M2 than at M1 in accordance with the average metal oxygen distances at these positions (see Table 3 and Section II).

Because the dipolar contribution to the magnetic hyperfine field at the chromium site is negligible, the difference between the experimental magnetic hyperfine field (Eq. (4)) and the orbital HF field (Eq. (5)) may then be attributed to the core polarization HF field

$$H_{\mathrm{cp}}^{\mathrm{HF}} = -\frac{AS}{g_I \mu_I} - H_{\mathrm{orb}}^{\mathrm{HF}}. \qquad (6)$$

In contrast to the orbital the core polarization hyperfine field has been observed to be independent from the atomic distances within the host lattice. Regarding the limits of error of the parameters A at M1 and M2, this is in qualitative agreement with the values obtained for $H_{\mathrm{cp}}^{\mathrm{HF}}$ (Table 3) at these positions.

From Table 3 it can be noted that the parameter A seems to be slightly smaller at M1 than at M2. This may be interpreted such that the covalency of the Cr–O bond at M1 is slightly larger than at M2, in accordance with the average M1–O and M2–O distances in forsterite. To estimate the covalent contribution to the Cr–O bond in forsterite, Paulings definition of the covalency, c, is used [10]. According to that, the definition contains two assumptions:

i) A general relationship exists between the electronegativity difference $X_A - X_B$ and the covalency of an A–B bond.

ii) The gauge curve can be constructed by taking the electric dipole moments of the hydrogen halides as representative for the ionic character ($i = 1 - c$) in these compounds.

The gauge curve proposed by Hannay and Smith [11]

$$c = 1 - 0.16(X_A - X_B) - 0.035(X_A - X_B)^2 \qquad (7)$$

Table 3. Hyperfine splitting parameter A deduced magnetic hyperfine fields of $^{55}Mn^{2+}$, $^{55}Fe^{3+}$ and $^{53}Cr^{3+}$ at M1 and M2 positions in Mg_2SiO_4. The signs of the magnetic HF fields were not experimentally determined.

Center	Position	A / 10^{-4} cm^{-1}	$g_I\beta_I$ / 10^{-24} erg/G	I	S	$AS/g_I\beta_I$ / kG	$H^{\mathrm{HF}}/2S$ / kG	Δg_{av}	$H_{\mathrm{orb}}^{\mathrm{HF}}/2S$ / kG	$H_{\mathrm{cp}}^{\mathrm{HF}}/2S$ / kG
$^{55}Mn^{2+}$	M2	84.1[a]	6.9495	5/2	5/2	601	(−) 120.2	−[c]	—	(−) 120
$^{57}Fe^{3+}$	M1	9.9 ± 0.4[b]	0.9115	1/2	5/2	539	(−) 107.8	−[c]	—	(−) 107
$^{57}Fe^{3+}$	M2	10.3 ± 0.2[b]	0.9115	1/2	5/2	561,1	(−) 112,2	−[c]	—	(−) 112
$^{53}Cr^{3+}$	M1	15.5 ± 1.7	1.5944	3/2	3/2	289.6	(−) 96.5	− 0.031	(−) 7.7	(−) 89
$^{53}Cr^{3+}$	M2	16.5 ± 2.1	1.5944	3/2	3/2	308.3	(−) 102.7	− 0.041	(−) 10.1	(−) 92

[a] Value taken from Gaite [2]. [b] Values taken from Niebuhr [1].
[c] The deviation of the $Fe^{3\pm}$ and $Mn^{2\pm}$ g-values from 2.0023 is negligible [5].

can then be used to calculate the degree of covalency. Taking the electronegativities $X_{A,B}$ from Gordy and Thomas [12], from Eq. (7) an average covalency of apparently 10% was obtained for the Cr–O bond in forsterite.

For comparison, the corresponding magnetic hyperfine parameters A obtained for the ions $^{57}Fe^{3+}$ and $^{55}Mn^{2+}$ in forsterite are also listed in Table 3. The hyperfine interaction and covalency of Mn^{2+} ions in different hosts were already discussed in detail by Simánek and Müller [7], and van Wieringen [8]. According to that, the hyperfine constant decreases with increasing covalency. At M2 in forsterite the $^{55}Mn^{2+}$-HF constant is isotropic and yields $84.5 \cdot 10^{-4}$ cm^{-1} [2]. Comparing this value with published data [7, 8] the covalent contributions to the Mn–O bond in forsterite turns out to be roughly 10%.

Likewise, the hyperfine constants of $^{57}Fe^{3+}$ at M1, M2 and the silicon position in forsterite have already been discussed by Niebuhr [1]. Their values for an octahedral and tetrahedral coordination agree with corresponding literature [13]. For the two octahedrally coordinated M1 and M2 sites one obtains a covalent contribution to the Fe–O bond of roughly 13%. However, as found for the Cr–O bonds, the covalency of the Fe–O bonds also seems to increase slightly with decreasing metal oxygen distance. Actually, the covalent contributions for the Mn–O and Fe–O bonds in forsterite were deduced from gauge curves given by Simanek and Müller [7] and Henning [13], respectively, and not calculated from Equation (7). However, the gauge curves are also based on the relation (7) of Hannay and Smith [11].

Conclusions

In summary, we establish that the ions Fe^{3+}, Mn^{2+}, and Cr^{3+} in their sixfold oxygen coordination in forsterite exhibit a covalent bonding of 10 to 15%, i.e. the bonding of these transition metal ions is not purely but mainly ionic. This may be interpreted such that the covalent contribution to the metal oxygen bonding is mainly dominated by the oxygens and less by properties of the transition metal ions themselves, like ionic radius and electron configuration. Further, the small variation of the HF-splitting parameters found for $^{53}Cr^{3+}$ at M1 and M2, and also for $^{57}Fe^{3+}$ at these positions [1] indicates that the HF-interaction varies with varying metal oxygen distances.

There are a series of methods like ESR, NMR, Compton scattering, Mössbauer and photoelectron spectroscopy to investigate covalency effects. However, to date it is still a problem to extract detailed information about the spin and charge distribution in the investigated complex from the experimental results, and to discuss this information with respect to the electronic structure of the complex. This problem is also valid for the above discussion, which gives only a qualitative interpretation of the investigated transition metal oxygen bonds in forsterite. For a more detailed discussion of this problem, additional experiments like, e.g., ENDOR measurements are necessary.

[1] H. Niebuhr, Elektronenspin-Resonanz von dreiwertigem Eisen in Forsterit. Habilitationsschrift, FB Geowissenschaften, Marburg 1976.
[2] J.-M. Gaite, Etude de Propriétés Locales dans les Cristaux de Basse Symétrie à l'Aide de la Résonance Paramagnétique Electronique d'Ions à l'Etat S. Dissertation, Orleans 1973.
[3] H. Rager, Phys. Chem. Minerals **1**, 371 (1977).
[4] J. R. Smyth and R. M. Hazen, Amer. Mineral. **58**, 588 (1973).
[5] A. Abragam and B. Bleaney, Electron Paramagnetic Resonance of Transition Metal Ions, Clarendon Press, Oxford 1970.
[6] A. J. Freeman and R. E. Watson, Hyperfine Interactions in Magnetic Materials, in: Magnetism Vol. IIa, Chapter 4. Editors: T. G. Rado and H. Suhl, Academic Press, New York 1965.
[7] E. Simánek and K. A. Müller, J. Phys. Chem. Solids **31**, 1027 (1970).
[8] J. S. van Wieringen, Disc. Faraday Soc. **119**, 118 (1955).
[9] R. M. Golding and W. C. Tennant, Mol. Physics **25**, 1163 (1973).
[10] L. Pauling, Die Natur der chemischen Bindung, Cornell University Press, Ithaca, N.Y. 1960.
[11] M. B. Hannay and C. F. Smyth, J. Amer. Chem. Soc. **68**, 171 (1946).
[12] W. Gordy and W. J. O. Thomas, J. Chem. Phys. **24**, 439 (1956).
[13] J. C. M. Henning, Physics Letters **24 A**, 40 (1967).